Catal Lett (2011) 141:1345–1354
DOI 10.1007/s10562-011-0653-8

Selective Catalytic Oxidation (SCO) of Ammonia to Nitrogen over Hydrotalcite Originated Mg–Cu–Fe Mixed Metal Oxides

Lucjan Chmielarz · Agnieszka Węgrzyn · Magdalena Wojciechowska · Stefan Witkowski · Marek Michalik

Received: 22 February 2011 / Accepted: 20 June 2011 / Published online: 2 July 2011

Abstract Mg–Cu–Fe oxide systems, obtained from hydrotalcite-like precursors, were tested as catalysts for the selective catalytic oxidation (SCO) of ammonia. Copper containing catalysts were active in low-temperature SCO processes; however, their selectivity to nitrogen significantly decreased at higher temperatures. The optimum composition of the catalyst to guarantee high activity and selectivity to N_2 was proposed. Temperature-programmed experiments, SCO catalytic tests performed with various contact times and additional tests on the samples in the selective catalytic reduction of NO with ammonia showed that the SCO process over the studied calcined hydrotalcites proceeds according to the internal SCR mechanism and oxidation of ammonia to NO is a rate-determining step in the low-temperature range.

Keywords Hydrotalcite-like materials · Selective catalytic oxidation of ammonia · Reaction mechanism

1 Introduction

The increasing problem of atmospheric pollution by various *N*-containing compounds, such as NO, N_2O, NO_2, and NH_3, has resulted in stricter regulations on their emissions. Many chemical processes have ammonia as a reactant or produce ammonia as a by-product (e.g., nitric acid and nitrogen fertilizer production, urea manufacturing, hydrodenitrification process, DeNOx process). The selective catalytic oxidation (SCO) of ammonia by oxygen to nitrogen and water vapour, according to the reaction given below, is one of the most promising methods for the removal of NH_3 from oxygen containing waste gases.

$$4\ NH_3 + 3\ O_2 = 2\ N_2 + 6\ H_2O$$

N_2O and NO are the main by-products of this process. Therefore, the effective SCO catalysts should operate at a relatively low-temperature range and additionally should result in the production of nitrogen and water vapour.

Various transition metal oxides including CuO, Fe_2O_3, Co_3O_4, MnO_2 MoO_3, V_2O_5 (e.g., [1–6]) were tested as catalysts for the SCO process. Among them the catalysts containing copper and/or iron were found to be some of the most interesting systems.

Recently, there have been a number of published studies on the use of Cu-containing catalysts for the SCO process. Copper oxide deposited on alumina, titania, and zeolites exchanged with copper were found to be active and selective catalysts for the low-temperature SCO process, however, their catalytic performance was significantly decreased by the presence of water vapour in the reaction mixture [7–10]. Hung [11] has shown high activity of a CuO/La_2O_3 oxide system obtained by the co-precipitation method, while Cui et al. [6] reported high activity and selectivity to nitrogen of the mesoporous CuO/RuO_2 catalysts obtained by a co-nano casting-replication method. On the other hand, saponite intercalated with silica pillars and modified with copper and iron were found to be active and selective catalysts for selective ammonia oxidation [12]. However, the Cu-modified clays were active at lower temperatures than the samples doped with iron.

L. Chmielarz (✉) · A. Węgrzyn · M. Wojciechowska · S. Witkowski
Faculty of Chemistry, Jagiellonian University, Ingardena 3, 30-060 Kraków, Poland
e-mail: chmielar@chemia.uj.edu.pl

M. Michalik
Institute of Geological Sciences, Jagiellonian University, Oleandry 2a, 30-063 Kraków, Poland

Our previous studies have shown that hydrotalcite-like materials are very interesting precursors of the catalysts for the SCO process [13]. Hydrotalcites, also called layered double hydroxides (LDHs), show the brucite-like network [$Mg(OH)_2$], where the octahedra of Mg^{2+}, six-coordinated to OH^-, form parallel layers. Some of the Mg^{2+} cations are replaced by trivalent ones (e.g., Al^{3+}) which result in an increase of the positive charge density of the layer. This net positive charge is compensated by anions (e.g., CO_3^{2-}, NO_3^-) which together with water molecules are located in the interlayer space. Furthermore, some of the Mg^{2+} as well as Al^{3+} ions can be replaced, respectively, by other di- (e.g., Cu^{2+}) and/or tri-valent (e.g., Fe^{3+}) cations. Calcination of the hydrotalcite precursors results in their decomposition and the formation of thermally stable mixed metal oxides characterized by a relatively high surface area and homogenous distribution of metal cations. Taking into account the properties mentioned above and additionally a large number of various metals, which can be incorporated into brucite-like layers, hydrotalcites are very promising materials for possible applications in catalysis. Our previous studies [13–15] have shown that catalysts obtained from Cu–Mg–Al hydrotalcites were active in the low-temperature range, but their selectivity to N_2 drastically decreased with an increase in the reaction temperature. On the other hand calcined Mg–Fe–Al hydrotalcite was less active but presented much higher selectivity to nitrogen. Therefore, a series of Cu–Mg–Fe hydrotalcite-like materials with the various ratio of Cu/Fe were synthesized and tested as catalysts for the SCO process. Another goal of the studies was the recognition of the reaction mechanism over the hydrotalcite derived catalysts.

2 Experimental

2.1 Catalysts Preparation

A series of Mg(II)Cu(II)Fe(III) hydrotalcite-like materials was prepared by the co-precipitation method using aqueous solutions of the following metal nitrates: $Mg(NO_3)_2{\cdot}6H_2O$ (Sigma), $Cu(NO_3)_2{\cdot}3H_2O$ (Merck) and $Fe(NO_3)_3{\cdot}9H_2O$ (POCh). A solution of NaOH (POCh) was used as a precipitating agent. The mixture of metal nitrate solutions was slowly added to a vigorously stirred aqueous solution containing a slight excess of Na_2CO_3 (POCh). The pH was maintained constant at 11.0 ± 0.2 by dropwise addition of NaOH solution. Precipitates were aged in a suspension at 60 °C for 30 min under vigorous stirring. In the next step the suspension was filtered, washed with distilled water and dried overnight at 100 °C. Finally, the prepared hydrotalcite-like materials were calcined at 600 °C for 12 h in an air atmosphere. The catalysts with the Mg:Cu:Fe molar ratios of 2:1:1, 2:0.75:1, 2:0.5:1, 2:0.25:1, and 2:0:1 were prepared. The samples were kept in a desiccator in order to avoid the reconstruction of the hydroxide structure.

2.2 Catalysts Characterization

The X-ray diffraction (XRD) patterns of as-synthesized and calcined hydrotalcite-like materials were recorded with a Philips X'Pert APD diffractometer using CuK_α radiation ($\lambda = 1.54056$ Å).

The surface areas of the calcined hydrotalcites were determined by the BET method using a Quantasorb Junior sorptometer (Ankersmit). Prior to nitrogen adsorption at −196 °C the samples were outgassed in a nitrogen atmosphere at 250 °C for 2 h.

The TPRed (temperature-programmed reduction) of the samples (30 mg) was carried out from room temperature to 1,100 °C with a linear heating rate of 5 °C/min. Measurements were performed in a fixed-bed flow micro reactor (i.d., 4.0 mm; bed height, 3 mm). Prior to the TPRed experiment, the samples were calcined at 600 °C for 12 h. The TPRed runs were carried out in a flow of 10 vol% of H_2 diluted in Ar (Messer) with a total flow rate of gas mixture of 6 mL/min. Evolving water was removed from effluent gas by means of a cold trap. The evolution of hydrogen was detected by micro volume TCD (Valco).

2.3 Catalytic Tests

The catalytic performance of calcined hydrotalcites in the selective catalytic oxidation of ammonia (SCO) has been studied under atmospheric pressure in a fixed-bed flow reactor (i.d., 7 mm; L, 240 mm). The reactant concentrations were continuously measured using a quadruple mass spectrometer (VG QUARTZ) connected to the reactor via a heated line. Prior to the reaction, each sample of the catalyst (100 mg) was outgassed in a flow of pure helium at 600 °C for 1 h. The composition of the gas mixture at the reactor inlet was $[NH_3] = 0.5$ vol%, $[O_2] = 2.5$ vol% and optionally $[H_2O] = 3.4$ vol%. Helium (grade 5) was used as balance gas. The total flow rate of the reaction mixture was 40 mL/min, while the space velocity was about 15,400 h^{-1}. Water vapour was introduced by passing the helium flow through a water saturator at elevated temperature. The reaction was studied at temperatures ranging from 50 to 450 °C. The intensities of the mass lines corresponding to all reactants and possible products were measured at a given temperature for at least 30 min after the reaction had reached a steady-state. The signal of the helium line served as the internal standard to compensate small fluctuations of the operating pressure. The sensitivity factors of analyzed lines were calibrated using commercial mixtures of gases. The possible changes in the molar flow

caused by NH_3 conversion were negligible in the diluted reaction mixtures. The differences between the reactor inlet and outlet molar flows of the reactants were used to determine conversion of the reactants.

Apart from the studies of the SCO process, calcined hydrotalcites were tested in the role of catalyst for the process of selective catalytic reduction of NO (NO-SCR). The catalytic experiments were performed in a fixed-bed flow reactor system, which was described above. The reactant concentrations were continuously measured using a quadruple mass spectrometer (VG QUARTZ) connected directly to the reactor outlet. Prior to the reaction, each sample (100 mg) of the catalyst was outgassed in a flow of pure helium at 600 °C for 30 min. The following composition of the gas mixture was used: $[NO] = [NH_3] =$ 0.25 vol%, $[O_2] = 2.5$ vol%. Helium was used as a balancing gas at a total flow rate of 40 mL/min.

2.4 Studies on the Reaction Mechanism

2.4.1 *Temperature-Programmed Desorption (NH_3–TPD) and Temperature-Programmed Surface Reaction (NH_3–TPSR)*

The interaction of the catalysts with ammonia was studied by temperature-programmed desorption of ammonia (NH_3–TPD) and temperature-programmed surface reaction (NH_3-TPSR). The measurements were performed in a flow micro reactor system equipped with a QMS detector (VG Quartz). Prior to the ammonia sorption the sample (100 mg) was outgassed in a flow of pure helium at 600 °C for 1 h. Subsequently, the micro reactor was cooled down to 70 °C and the sample was saturated in a flow (20 mL/min) of gas mixture containing 1 vol% of NH_3 diluted in helium for about 75 min. Then, the sample was purged in a flow of pure helium until a constant baseline level was attained (about 2 h). In the next step the temperature of the reactor was raised in the range of 70–600 °C with a linear heating rate of 10 °C/min in a flow of pure helium (NH_3–TPD) or in a flow of gas mixture containing 5 vol% of O_2 diluted in helium (NH_3–TPSR). The total flow rate in each case was 20 mL/min.

2.4.2 *SCO Catalytic Tests Performed with Various Space Velocities*

Catalytic tests were preformed using the experimental system described above. Prior to the reaction each sample of the catalyst was outgassed in a flow of pure helium at 600 °C for 1 h. Experiments were done for various amounts of catalyst (25, 50, and 100 mg) in the range of 100–450 °C. The composition of the gas mixture at the reactor inlet was $[NH_3] = 0.5$ vol%, $[O_2] = 2.5$ vol% and $[He] = 97$ vol%. Total flow rate of the reaction mixture was 40 mL/min, while space velocities were about 15,400; 30,800; and 61,600 h^{-1}.

3 Results and Discussion

The sample codes as well as their cationic ratios and BET surface areas are presented in Table 1, while the X-ray diffractograms of the dried and calcined hydrotalcites are presented in Fig. 1.

All precursors exhibit the typical crystalline hydrotalcite-like structure belonging to the space group R3 m [16]. Cell parameters were calculated using a position of 110 reflection: $a = 2(d_{110})$ and positions of basal reflections: $c = [3(d_{003}) + 6(d_{006})]/2$. The parameter a corresponds to the cation–cation distance within the brucite-like layer, while the parameter c is related to the thickness of the brucite-like layer and the interlayer distance [16]. Additionally, crystal sizes were calculated from the Scherrer equation $D = 0.89\ \lambda/\beta\ \cos\theta$, where D is the crystallite size, λ—the X-ray wavelength, β—the line broadening and θ—the Bragg angle. Calculated values were shown in Table 2.

The cell parameter a for the $Mg_2Cu_0Fe_1$ sample is typical for a mixed magnesium-iron layered double hydroxide with M^{II}/M^{III} ratio close to two [17] and in which trivalent cation positions are occupied by Fe^{3+}. Intermetallic distance increases slightly for the series of the copper-doped hydrotalcite-like samples. The result is due to the bigger radius of Cu^{2+} cations (0.069 nm) than Mg^{2+} (0.065 nm) and Fe^{3+} (0.064 nm) introduced into the layers. However, for Cu-rich phases no further increase of parameter a was observed and in the case of $Mg_2Cu_1Fe_1$ sample small additional reflections were detected, probably corresponding to tenorite, CuO. It is well known that for octahedral coordinated cations such as Ni^{2+} or Cu^{2+} a strong Jahn–Teller effect may take place. Distortions caused by incorporation of high amounts of Cu cations cannot be accommodated by a crystalline lattice. The formation of additional Cu-phases is observed, i.e., $Cu(OH)_2$ which transforms into CuO upon aging treatment. A similar

Table 1 Composition and BET surface area of calcined hydrotalcites

Codes of the samples before calcination	Codes of the calcined samples	Mg/Cu/Fe molar ratio	BET surface area (m^2/g)
$Mg_2Cu_1Fe_1$	HT-600-$Mg_2Cu_1Fe_1$	2/1/1	43
$Mg_2Cu_{0.75}Fe_1$	HT-600-$Mg_2Cu_{0.75}Fe_1$	2/0.75/1	37
$Mg_2Cu_{0.5}Fe_1$	HT-600-$Mg_2Cu_{0.5}Fe_1$	2/0.5/1	50
$Mg_2Cu_{0.25}Fe_1$	HT-600-$Mg_2Cu_{0.25}Fe_1$	2/0.25/1	54
$Mg_2Cu_0Fe_1$	HT-600-$Mg_2Cu_0Fe_1$	2/0/1	56

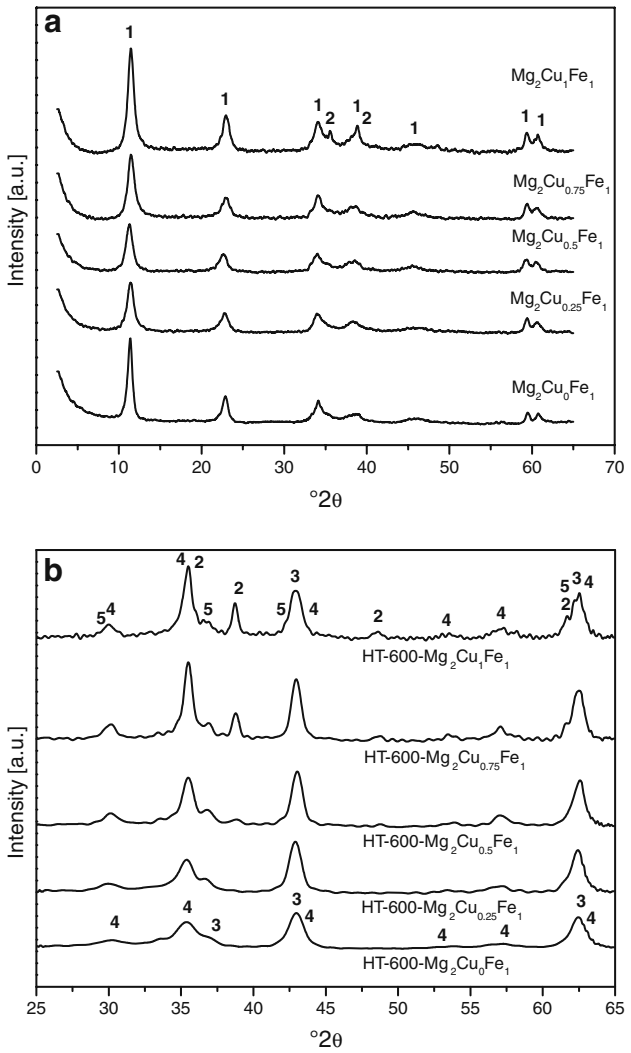

Fig. 1 X-ray diffraction patterns for hydrotalcite-like catalysts' precursors (**a**) and mixed metal oxide catalysts (**b**); *1*—hydrotalcite, *2*—tenorite, CuO, *3*—periclase, MgO, *4*—magnesioferrite, $MgFe_2O_4$, *5*—cuprite, Cu_2O

Table 2 Structural parameters of hydrotalcite-like catalysts' precursors

Codes of the samples before calcination	Cell parameter *a* (nm)	Crystallite size *Da* (nm)	Cell parameter *c* (nm)	Crystallite size *Dc* (nm)
$Mg_2Cu_1Fe_1$	0.3110	28	2.318	17
$Mg_2Cu_{0.75}Fe_1$	0.3110	31	2.317	15
$Mg_2Cu_{0.5}Fe_1$	0.3115	25	2.357	16
$Mg_2Cu_{0.25}Fe_1$	0.3110	33	2.333	16
$Mg_2Cu_0Fe_1$	0.3105	35	2.335	23

effect of Cu doping was also reported for a Co–Cu–Fe hydrotalcite series [18].

It was reported before that the interlayer distance is also affected by the introduction of copper [18, 19]. Basal spacing depends on the interlayer water content, the amount, size, orientation, and charge of the anion located between the brucite-like layers [17]. The values obtained in the study of about 2.3 nm are typical for hydrotalcites containing carbonate as the interlayer anion; however, parameter *c* increases for small Cu-concentrations ($Mg_2Cu_{0.5}Fe_1$). This result can be attributed to a decrease in the electrostatic interactions between the layer and the interlayer network when another divalent cation is introduced into the structure. Further introduction of Cu results in contraction of basal spacings. Possible phase segregation, as described above, may again cause an increase of the charge density in the layers and a subsequent increase in the attractive electrostatic force. Introduction of Cu^{2+} and distortions within the hydrotalcite structure resulted in broadening of the reflections in all Cu-doped samples. Consequently, crystallinity of those materials is lower in comparison to Mg/Fe hydrotalcite.

The layered structure of the calcined samples was destroyed upon heating. The mixture of oxide and spinel phases was identified in all samples. The calcined Mg–Fe hydrotalcite-like sample (HT-600-$Mg_2Cu_0Fe_1$) consisted of poor-crystalline periclase (MgO) and magnesioferrite ($MgFe_2^{III}O_4$) [20, 21], however, another spinel phase ($Fe^{II}Fe_2^{III}O_4$) [20, 22] also cannot be excluded. Incorporation of increasing amounts of Cu resulted in the formation of at least four different phases in Mg–Cu–Fe oxide catalysts. Also crystallinity increases gradually with Cu-concentration. The reflections at 36.4, 42.3, 61.3, and 29.6°2θ observed in all the Cu-doped catalysts can be attributed to cuprite (Cu_2O) [20, 23]. Formation of tenorite (CuO), on the other hand, depends on high copper concentration. Sharp reflections, partially overlapped by the other phases, were observed at 35.6, 38.7, 48.8, and 61.6°2θ. This result can be attributed to the temperature-induced reduction which occurs easily for highly dispersed CuO. Besides periclase and magnesioferrite, the presence of other iron oxides is also possible. However, no traces of cuprospinel (Cu^{II}, Mg)$Fe_2^{III}O_4$ or $Cu^{II}Fe_2^{III}O_4$ were found [24].

TPRed profiles of the calcined hydrotalcite samples are presented in Fig. 2. Sharp peaks at about 190–195 °C and 200–205° (marked in Fig. 2 as α and β) were found for the copper containing samples. The α peak is related to the reduction of highly dispersed copper oxide species, which include isolated copper ions and small two- and three-dimensional clusters [25–28]. The β peak is associated with reduction of bulk-like CuO phases that include large clusters and bulk CuO. Therefore, it is not surprising that the intensity of the β peak increased with an increase in the copper content. The TPRed peaks related to reduction of iron species appeared at temperatures 460–480 °C (peak γ) and 540–620 °C (peak δ). XRD studies have shown that iron could be present in the form of $MgFe_2^{III}O_4$ and/or

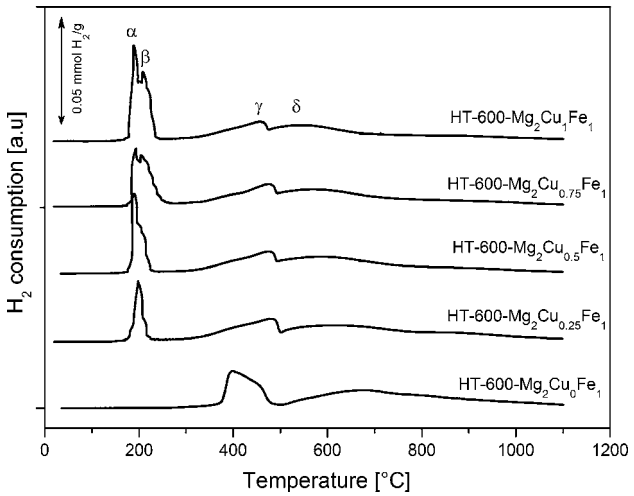

Fig. 2 Temperature-programmed reduction (TPRed) of mixed metal oxide catalysts. Conditions: 30 mg catalyst, 10% H_2 diluted in Ar, flow rate of 6 mL/min, linear heating rate of 5 °C/min

$Fe^{II}Fe_2^{III}O_4$, however, distinction between these two spinel oxides was not possible by the XRD method due to very similar diffraction patterns. More information concerning the contribution of both these spinel phases in the catalysts can be obtained from TPRed experiments. Assuming that both spinel oxides are reduced by hydrogen in two steps [28, 29] the processes could be presented in the form of the following equations:

$$MgFe_2^{III}O_4 \rightarrow MgO + 2\ FeO \rightarrow MgO + 2\ Fe$$

$$Fe^{II}Fe_2^{III}O_4 \rightarrow 3\ FeO \rightarrow 3\ Fe$$

Therefore for the reduction of iron in $MgFe_2^{III}O_4$ the ratio of hydrogen consumption in the first and second step is 1:2, while for the reduction of $Fe^{II}Fe_2^{III}O_4$ it is 1:3. Analysis of the TPRed results showed that the hydrogen consumption ratio for both steps was 1:2.12 and 1:2.14 for the samples with the lower Cu-content (HT-600-$Mg_2Cu_{0.25}Fe_1$ and HT-600-$Mg_2Cu_{0.5}Fe_1$, respectively) and 1:2.64 and 1:2.27 for the samples with the higher Cu-content (HT-600-$Mg_2Cu_{0.75}Fe_1$ and HT-600-$Mg_2Cu_1Fe_1$, respectively), while the ratio of 1:2.42 was found for the sample without copper (HT-600-$Mg_2Cu_0Fe_1$) Therefore, it could be concluded that both spinel phases are present in the samples but their contribution is varied.

Calcined hydrotalcites were tested as catalysts for the selective oxidation of ammonia. Nitrogen and water vapour are desired products of this process, while nitrogen oxides are undesired by-products. Results of activity studies are presented in Fig. 3. Oxidation of ammonia started at 225–250 °C, while temperatures 425–450 °C were necessary for the complete ammonia conversion in the reaction mixture. An exception was the catalyst without copper (HT-600-$Mg_2Cu_0Fe_1$), which was found to be significantly

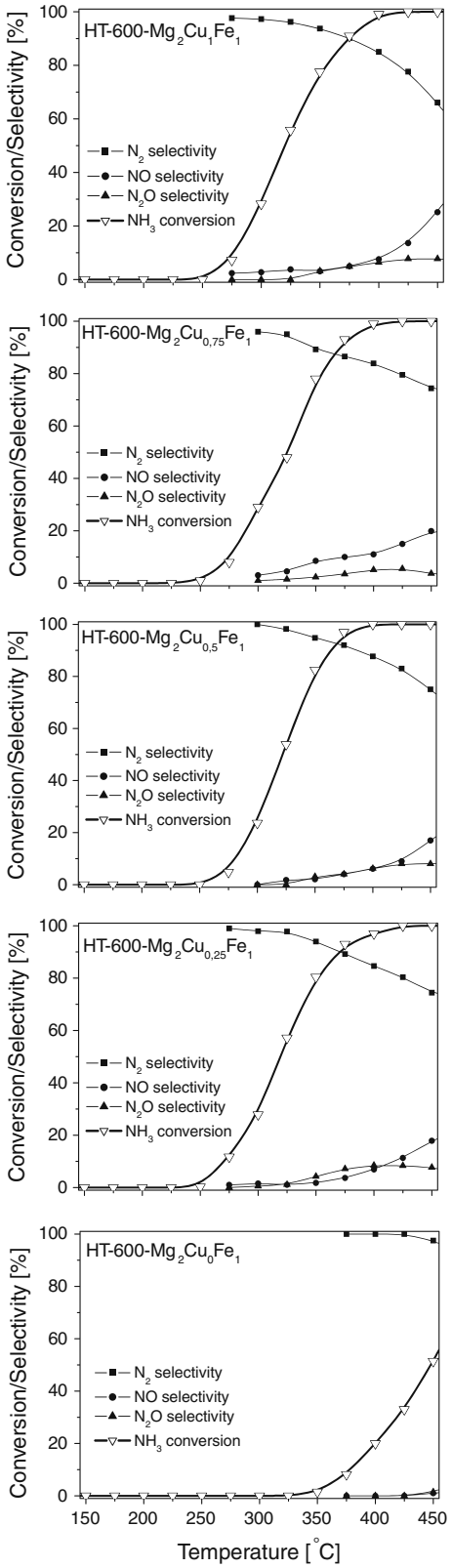

Fig. 3 Selective catalytic oxidation of ammonia over hydrotalcite derived catalysts. Conditions: 100 mg catalyst, $[NH_3] = 0.5\%$, $[O_2] = 2.5\%$, [He] = 97%, total flow rate = 40 mL/min

less active. For this catalyst, ammonia oxidation started at 325 °C and its complete removal from the reaction mixture was not obtained in the studied temperature range. Therefore, it could be concluded that the presence of copper activated catalysts for the low-temperature ammonia oxidation is essential. On the other hand, the copper content in the samples only slightly differentiated their catalytic activity. N_2, NO, and N_2O were the only detected *N*-containing reaction products. For all the catalysts, nitrogen was the dominating product in the studied temperature range; however, its concentration decreased with rising reaction temperature. An opposite effect was observed for the evolution of NO. Selectivity to N_2O was rather low and did not exceed 12% in the studied temperature range. Catalysts composition strongly influenced their selectivity to *N*-containing products. For the catalysts with the highest Cu-loading (HT-600-$Mg_2Cu_1Fe_1$) an increase in NO selectivity and decrease in N_2 selectivity at higher temperatures was more significant in comparison to the other Cu-containing samples. Taking into account both high activity and selectivity to nitrogen the best results were presented by the HT-600-$Mg_2Cu_{0.5}Fe_1$ catalyst, which was able to completely oxidise ammonia in the reaction mixture at 400 °C with a selectivity to nitrogen of about 88%.

For the HT-600-$Mg_2Cu_{0.5}Fe_1$ catalyst additional catalytic tests with a gas mixture containing water vapour were done (Fig. 4). The temperature of complete ammonia conversion increased by about 25 °C after the introduction of water vapour into the reaction mixture (Fig. 4a). Also an increase in NO selectivity and decrease in N_2 selectivity was observed for the process performed in the presence of wet reaction mixture. Figure 4b presents stability tests performed for the HT-600-$Mg_2Cu_{0.5}Fe_1$ catalyst in a flow of dry and wet reaction mixture. The introduction of water vapour into the reaction mixture only slightly decreased ammonia conversion and selectivity to nitrogen. However, switching from wet to dry reaction mixture resulted in an increase of these parameters to the former level. Therefore, it could be concluded that introduction of water vapour into the reaction mixture did not result in the permanent deactivation of the catalyst. It should be also noted that any significant depletion in conversion and selectivity was not observed within the period of prolonged activity tests with wet nor dry reaction mixture (Fig. 4b). Comparing the obtained results with that reported in the scientific literature it could be concluded the studied catalyst is significantly less sensitive to the presence of water vapour than other active Cu-doped catalysts of the SCO process (e.g., Cu/TiO_2 [8], Cu/Al_2O_3, CuY [9, 10]).

The interaction of ammonia molecules with the catalysts' surface was studied by temperature-programmed methods. The results of temperature-programmed desorption of ammonia (NH_3–TPD) are shown in Fig. 5. For all the samples, apart from ammonia desorption, also the evolution of N_2 and N_2O was detected. Nitrogen was formed at temperatures below 400 °C and its evolution is represented by desorption curves with different shapes. For HT-600-$Mg_2Cu_{0.5}Fe_1$ the evolution of nitrogen proceeded in one stage, while in the case of the other catalysts at least two peaks of nitrogen evolution were detected. For the Cu-containing catalysts the evolution of N_2O was observed in the temperature range of 150–400 °C, while the formation of nitrous oxide over HT-600-$Mg_2Cu_0Fe_1$ was detected at higher temperatures and proceeded in two stages 260–375 °C and 415–510 °C. This effect is probably related to the presence of strongly chemisorbed ammonia on the surface of the HT-600-$Mg_2Cu_0Fe_1$ sample.

The evolution of N_2 and N_2O that assisted ammonia desorption is related to the partial oxidation of ammonia by lattice oxygen of the catalysts. Therefore, lattice oxygen seems to be able to directly oxidize ammonia.

Figure 6 presents the results of NH_3–TPSR measurements. Apart from ammonia, evolution of N_2, N_2O, and NO was also detected. A significant amount of desorbed ammonia suggests that the majority of chemisorbed NH_3 molecules are not involved in the low-temperature oxidation. The evolution of nitrogen and nitrous oxide for all the copper containing catalysts occurred at temperatures below

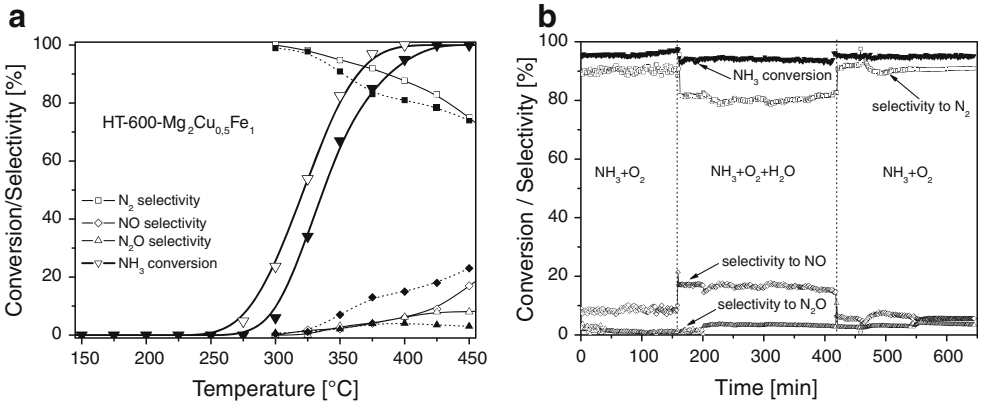

Fig. 4 Selective catalytic oxidation of ammonia over HT-600-$Mg_2Cu_{0.5}Fe_1$ catalyst. Conditions: 100 mg catalyst, $[NH_3] = 0.5\%$, $[O_2] = 2.5\%$, ($[H_2O] = 3.4\%$), He = balance, total flow rate = 40 mL/min. **a** Studies performed in polythermal conditions in flow of dry (*empty symbols*) and wet (*full symbols*) reaction mixture; **b** Studies performed at 400 °C with wet and dry reaction mixture

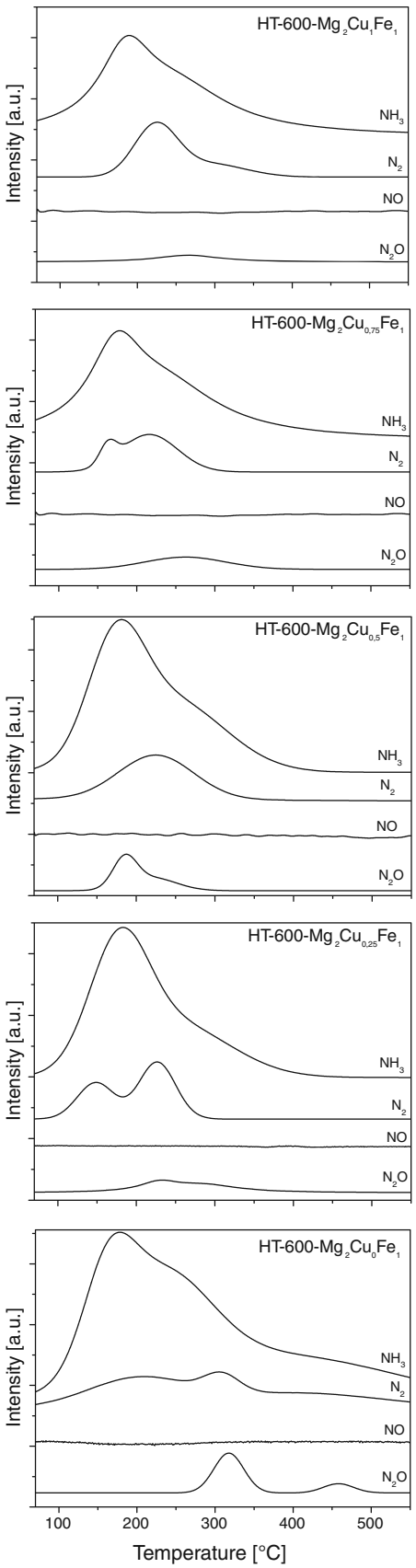

◀ **Fig. 5** Results of temperature-programmed desorption of NH_3 (NH_3–TPD) obtained for hydrotalcite derived catalysts. Conditions: 100 mg catalyst, adsorption: 70 °C, 1% NH_3 diluted in He, flow rate = 20 mL/min, desorption: flow of pure He = 20 mL/min, linear heating rate of 10 °C/min

400 °C. The evolution of N_2O from the HT-600-$Mg_2Cu_0Fe_1$ sample, similarly to NH_3–TPD, was detected at higher temperatures and proceeded in two, well resolved stages. The evolution of NO was the main difference between the results of NH_3–TPD and NH_3–TPSR. Nitric oxide was produced for all the samples in the temperature range of 350–500 °C.

Three major reaction mechanisms have been proposed for the SCO process over various types of catalysts. The first mechanism, which is often called the imide mechanism, was proposed by Zawadzki [30]. In the first step ammonia is oxidized with the formation of imide (NH), then the imide species react with molecular oxygen (O) to form the nitrosyl (HNO) intermediate, which in the next step reacts with imide resulting in the formation of N_2 and H_2O. N_2O is formed by the reaction of two nitrosyl species, while the reaction between NH and O_2 leads to NO. According to this mechanism, dissociation of O_2 and formation of active atomic oxygen species (O) is the key reaction step.

On the other hand, in our studies the oxidation of ammonia into N_2 and N_2O took place at a similar temperature range in the presence (NH_3–TPSR) or absence (NH_3–TPD) of gaseous oxygen (O_2). Therefore, it seems that the formation of active atomic oxygen species (O) by dissociation of O_2 did not occur over the studied catalysts and the evolution of N_2 and N_2O involved the reaction of ammonia with the lattice oxygen.

The second mechanism, called the hydrazine mechanism (e.g., [31, 32]), involves oxidation of ammonia to amide (NH_2) species by atomic oxygen (O), and subsequently the formation of hydrazine-type intermediates (N_2H_4). In the next step N_2H_4 is oxidised by O_2 to N_2 and/or N_2O. It should be noted that also in this case active oxygen species play an important role in the reaction mechanism.

The third mechanism, also called "internal" selective catalytic reduction (iSCR) (e.g., [13, 33, 34]) consists of two main steps. In the first step ammonia is oxidised to NO:

$$4\ NH_3 + 5\ O_2 \rightarrow 4\ NO + 6\ H_2O \quad (1)$$

While, N_2 and N_2O are formed in the subsequent reactions between NO and ammonia, which were not consumed in the process 1:

$$4\ NO + 4\ NH_3 + O_2 \rightarrow 4\ N_2 + 6\ H_2O \quad (2a)$$

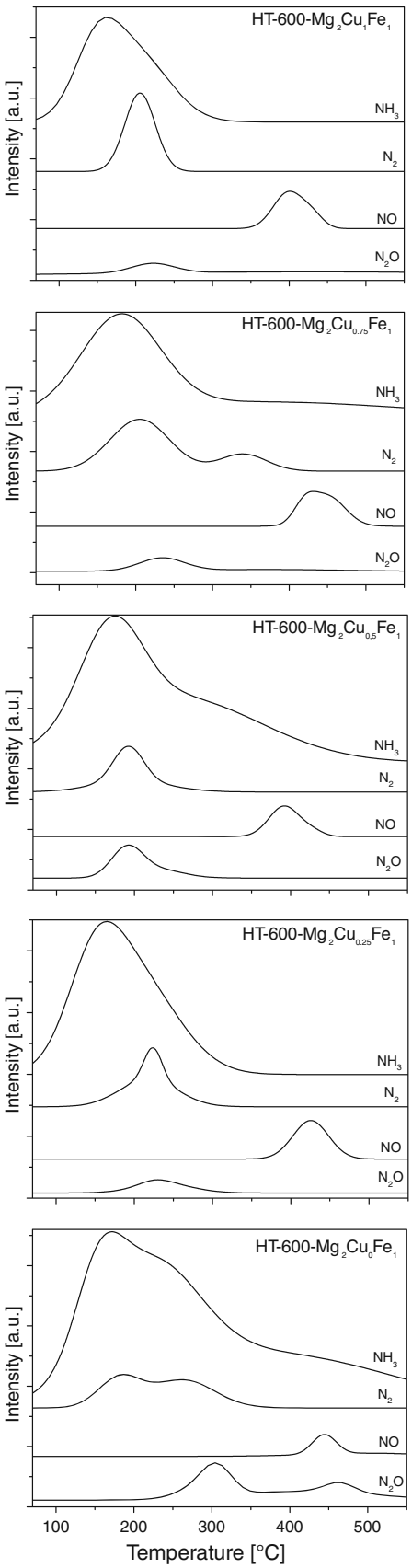

◀ **Fig. 6** Results of temperature-programmed surface reaction (NH_3–TPSR) obtained for hydrotalcite derived catalysts. Conditions: 100 mg catalyst, adsorption: 70 °C, 1% NH_3 diluted in He, flow rate = 20 mL/min, desorption: 5% O_2 diluted in He, flow rate = 20 mL/min, linear heating rate of 10 °C/min

$$4\ NO + 4\ NH_3 + 3\ O_2 \rightarrow 4\ N_2O + 6\ H_2O \qquad (2b)$$

If the process of ammonia oxidation proceeds according to the iSCR mechanism, the studied catalysts should also be active in the selective catalytic reduction of NO with ammonia (NO-SCR). Results of the studies of NO-SCR reaction are presented in Fig. 7. All the Cu-containing samples were catalytically active in the low-temperature range, however, at temperatures above 300 °C intensive ammonia oxidation drastically decreased the effectiveness of NO reduction. The HT-600-$Mg_2Cu_0Fe_1$ catalyst (without copper) was active at temperatures above 350 °C. It should be noted that ammonia oxidation in the SCO process over the copper containing catalysts started at about 225 °C (Fig. 2), while conversion of NO on the NO-SCR process

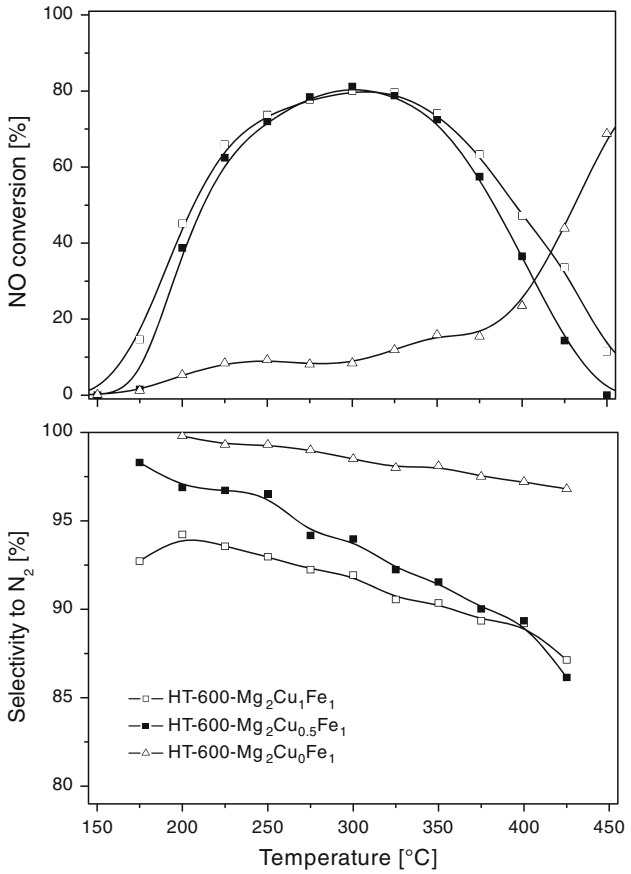

Fig. 7 Selective catalytic reduction of NO with ammonia over hydrotalcite derived catalysts. Conditions: 100 mg catalyst, $[NH_3] = 0.25\%$, $[NO] = 0.25\%$, $[O_2] = 2.5\%$, $[He] = 97\%$, total flow rate = 40 mL/min

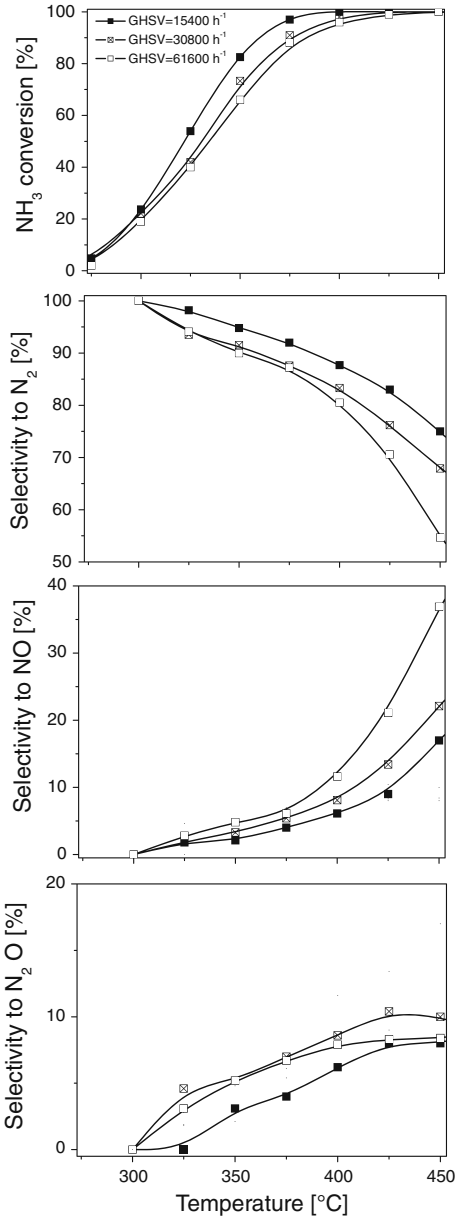

Fig. 8 Effect of space velocity (SV) on activity and selectivity of HT-600-$Mg_2Cu_{0.5}Fe_1$ catalyst in the SCO process. Conditions: 25, 50 or 100 mg catalyst, $[NH_3] = 0.5\%$, $[O_2] = 2.5\%$, He = balance, total flow rate = 40 mL/min

(Fig. 7) was observed at temperatures lower by about 75 °C. If we assume the iSCR mechanism of the SCO process is correct, it seems that oxidation of ammonia into NO (reaction 1) is a rate-determining step in the low-temperature range.

If the process of ammonia oxidation proceeds according to the sequence of the reactions presented above (iSCR mechanism) the distribution of products should depend on the space velocity (SV) of the process. For the experiment performed with lower SV (longer contact time) the increased selectivity to N_2 and N_2O is expected, while an increase in SV (shorter contact time) should promote the higher selectivity to NO. Figure 8 presents the results of the catalytic tests performed for the various space velocities. An increase in SV shifted the ammonia conversion curves into higher temperatures as well as decreased selectivity to nitrogen and increased selectivity to nitric oxide. Selectivity to nitrous oxide was rather low and only slightly affected by the changes in space velocity. The obtained results prove that the process of ammonia oxidation proceeds according to the sequence of the reactions 1, 2a, or 2b. This hypothesis is also supported by the results of NH_3–TPSR experiments. The evolution of NO was observed only in the high temperature range (Fig. 6), in which there was no chemisorbed ammonia able to convert nitric oxide to N_2 or N_2O.

4 Conclusions

Calcined Mg–Cu–Fe hydrotalcites were found to be active catalysts for the selective oxidation of ammonia. Activity of these catalysts depended on their chemical composition. The Cu-containing catalysts were active at lower temperatures and were less selective to nitrogen than the sample without copper (HT-600-$Mg_2Cu_0Fe_1$). Optimum composition of the catalysts guaranteeing high activity and selectivity to N_2 was proposed. The studies of the reaction mechanism showed that the process of ammonia oxidation over the hydrotalcite derived catalysts proceeds according to the internal selective catalytic reduction mechanism (iSCR).

Acknowledgments Authors are grateful to Krzysztof Kiper and Tony Robinson for proofreading of the manuscript.

References

1. Olofsson G, Hinz A, Anderson A (2004) Chem Eng Sci 59:4113
2. Li Y, Armor JN (1997) Appl Catal B 13:131
3. Amblard M, Burch R, Southward BWL (1999) Appl Catal B 22: L159
4. Sobczyk PD, Hensen EJM, de Jong AM, van Santen AS (2003) Top Catal 23:109
5. Long RQ, Yang RT (2002) Catal Lett 78:353
6. Cui X, Zou J, Ye Z, Chen H, Li L, Ruan M, Shi J (2010) J Catal 270:310
7. Lenihan S, Curtin T (2009) Catal Today 145:85
8. He S, Zhang C, Yang M, Zhang Y, Xu W, Cao N, He H (2007) Sep Purif Technol 58:173
9. Gang L, Grondelle J, Anderson BG, Santen RA (1999) J Catal 186: 100

10. Gang L, Anderson BG, Grondelle J, Santen RA (2000) Catal Today 61:179
11. Hung C-M (2009) Powder Technol 196:56
12. Chmielarz L, Kuśtrowski P, Drozdek M, Dziembaj R, Cool P, Vansant EF (2007) Catal Today 119:181
13. Chmielarz L, Kuśtrowski P, Rafalska-Łasocha A, Dziembaj R (2005) Appl Catal B 58:235
14. Chmielarz L, Kuśtrowski P, Rafalska-Łasocha A, Majda D, Dziembaj R (2002) Appl Catal B 35:195
15. Chmielarz L, Kuśtrowski P, Rafalska-Łasocha A, Dziembaj R (2003) Thermochim Acta 395:225
16. Węgrzyn A, Rafalska-Łasocha A, Majda D, Dziembaj R, Papp H (2010) J Therm Anal Calorim 99:443
17. Sanchez-Cantu M, Perez-Diaz LM, Maubert AM, Valente JS (2010) Catal Today 150:332
18. Iglesias AH, Ferreira OP, Gouveia DX, Souza Filio AG, de Paiva Mendel JAC, Filio J, Alves OL (2005) J Solid State Chem 178: 142
19. Carja G, Nakamura R, Niiyama H (2002) Appl Catal A 236:91
20. Downs RT (2006) The RRUFF project: an integrated study of the chemistry, crystallography, Raman and infrared spectroscopy of minerals. In: Program and abstracts of the 19th general meeting of the international mineralogical association in Kobe, Japan. O03-13
21. O'Neill HSC, Annersten H, Virgo D (1992) Am Miner 77:725
22. Blesa MC, Amador U, Moran E, Menendez N, Tornero JD, Rodriguez-Carvajal J (1993) Solid State Ion 63:429
23. Hafner SS, Nagel S (1983) Phys Chem Miner 9:19
24. Estrella M, Barrio L, Zhou G, Wang X, Wang Q, Wen W, Hanson JC, Frenkel AI, Rodriguez JA (2009) J Phys Chem C 113: 14411
25. Kim S-K, Kim K-H, Ihm S-K (2007) Chemosphere 68:287
26. Chary KVR, Seela KK, Ramakanth DNP (2008) Catal Commun 9:75
27. Dow W-P, Wang Y-P, Huang T-J (2000) Appl Catal A 190:25
28. Balasamy RJ, Khurshid A, Al-Ali AAS, Atanda LA, Legata K, Asamoto M, Yahiro H, Nomura K, Sano T, Takehira K, Al-Khattaf SS (2010) Appl Catal A 390:225
29. Holgado MJ, Rivers V, Sanroman MS, Malet P (1996) Solid State Ion 92:273
30. Zawadzki J (1950) Disc Faraday Soc 8:140
31. Amores JMG, Escribano VS, Ramis G, Busca G (1997) Appl Catal B 13:45
32. Darvell LI, Heiskanen K, Jones JM, Ross AB, Simell P, Williams A (2003) Catal Today 81:681
33. Qi G, Gatt JE, Yang RT (2004) J Catal 226:120
34. Zhang L, He H (2009) J Catal 268:18